Numerical Study of Thermal Plume in Corner Walls with Smoke Movement in Fire by Means of the Standard k-ε Model

TETSUO HARA and MUTSUMI YOKOI
Design Division, Taisei Corporation
1-25-1 Nishi-Shinjuku, Shinjuku-ku,
Tokyo 163-0606, Japan
E-mail: hara@arch.taisei.co.jp,
yokoi@arch.taisei.co.jp

SHINSUKE KATO
Institute of Industrial Science,
University of Tokyo
4-6-1 Komaba, Meguro-ku,
Tokyo 153-8505, Japan
E-mail: kato@iis.u-tokyo.ac.jp

ABSTRACT

The main purpose of this study is examination of the accuracy and the reliability of numerical simulations of a plume in corner walls in a view toward practical applications to the simulation of fire-safety planning. Corner plumes are computed numerically using the standard k-ε model and results are compared with model experiments. Three fire source locations are considered: (a) at, (b) close to, and (c) away from the corner. Dependence on divided mesh systems, the difference between compressible and incompressible flow solutions, and the sensitivity of the initial values of k and ε on results are investigated. The simulation predicts successfully entrainment of the corner plume.

Key words: CFD, Smoke Movement, Standard k-ε Model, Corner Plumes, Mesh Division

1. INTRODUCTION

In predicting the fire smoke movement, analysis on thermal-plume behavior acting as the smoke source of fire is essential. Much research attention has been directed toward free plume which has no spatial constraints[1]. As the location of the fire source approaches a wall, the flow pattern of plume changes and the flow tends to adhere to the wall. Since the amount of air supply to the plume on the wall side is cut compared to an open side, pressure near the wall drops, driving the central axis of the flow to tilt toward the wall. When there is more than one wall to form a corner, this character appears more clearly due to the confinement effect of the corner.

In the realworld fire, a fire started near a corner of the room often spreads along the wall toward the ceiling by generating flame and smoke. Heat from the fire gets concentrated at the corner due to the confinement effect arising from the walls adjoining at the right angle. This intensifies radiation heat transfer to the walls adjoining at the right angle and creates an area of high temperature, a source of the fire growth.

The present study is motivated by critical need for predicting patterns of fire smoke movement in a plume near the corner, high fire hazard in the realworld fire. A CFD study of corner plume is performed using the standard k-ε model to access the accuracy of numerical predictions by comparing results with experimental measurements[2-4]. The following factors are considered in the analysis in an attempt to conduct a systematic comparison study with the measurement: 1) location of the fire source, 2) dividing pattern of the mesh, 3) compressibility vs. incompressibility of flow, and 4) the inflow values of k and ε of fire. The main purpose of the present work is sensitivity analysis for the horizontal distributions of temperature and velocity and the flow rate of a corner plume in order to yield useful information from the practical viewpoint.

2. PREVIOUS INVESTIGATIONS

Relative to studies on free plumes to be found in unconfined spaces, corner plumes have attracted less research effort. Cetegen, Zukoski and Kubota[5] measured entraining air to plume (generated by fire with a heat release rate of 60 kW and a diameter of 0.19 m) with the aid of a hood. They report the effect of external disturbances stemming from covering the side of a lower opening of the hood with a screen. Klote and Milke[6] determined the flow rate of entraining air to plume from a fire source adjacent to a wall. In this case, the flow rate is one-half the value of a virtual axisymmetric plume whose assumed heat release rate is twice that of the actual fire source. When the fire source is near the corner, it becomes one-quarter the flow rate of the virtual axisymmetric plume with a four-fold heat release rate of the actual fire.

Sugawa and others[7,8] investigated experimentally entrainment of air caused by fire at or near the corner, thereby examined relationships between the flame height and entraining air. They employ an experimental set-up consisting of a pair of walls forming a corner at the right-angled intersection and a propane gas-fed diffusion flame burner measuring 0.1 m × 0.1 m. In the experiment, the ratio of $S1$,distance between a wall to the burner, to $S2$, distance between the remaining wall to the burner, is varied for a series of the fire-source edge-length D: see **FIGURE** A-1 and refer also to **Note** 1 at the end of text. As the location of the square fire comes closer to the corner, entrainment of air is restricted due to the walls, leading to a reduced flow rate of plume compared to a free boundary condition. Based on the experimental results, they report two findings: First, when the fire is near the corner, the temperature drop in the height direction in fire flame starts at a higher location than that in an unconfined space. Trends in velocity are similar, but effects attributable to the difference in entrainment patterns caused by the wall above the fire reveal more distinctively than those in the entrainment at the fire-source level. Secondly, when the fire is positioned at the corner, the horizontal distributions of temperature and velocity exhibit conical patterns, similar to those seen in a free space, in the continuous flame region. In and beyond the intermittent flame region, on the other hand, iso-value contours resemble a group of right isosceles triangles whose right-angled edges correspond to the two walls. As the walls block incoming air from the two directions, flame, or the plume, is pushed against the walls due to the pressure difference in the horizontal direction and subsequently spread along the walls.

In the extensive research work on corner plume by Sugawa et al.[9-12] [see **Note 2**], the temperature and velocity distributions and the flow rate of plume are documented for various $S1/S2$ for a series of fire heat release rates. Quantitative measurement of a rise in the mass flow rate in plume is made using the experimental data.[12] and results are validated by employing concentration of CO_2 gas and its mass as measures. It is found that 1) the entrainment rate of plume decreases when either flame or the plume comes in contact with wall; 2) the mass flow rate of the plume m_p, serving as an indicator of an increase in entraining air, is proportional to $(Z+Z_0)^{5/3}$, [5] in a free space, accounting for compensation height of an virtual heat source Z_0. While, in the near-corner region where the plume senses the wall influence, it is proportional to $(Z+Z_0)^{1.0}$ [see **Note** 3]; 3) mass of CO_2 passing through the plume zone, m_{CO_2}, drops in proportion to $(Z+Z_0)^{-1.0}$ at the height where the corner exerts effect, corresponding to an increase in plume mass; and, 4) in corner plume, it was known that the flame height exhibits characteristics of a free space at $S/D = 2.0$, while in the entrainment rate the effects of the corner are evident up to S/D = 3.0 when the plume region is also included.

3. COMPUTATIONAL CONDITION OF CORNER PLUME

Numerical analysis of corner plume under the corresponding condition of the experiment of **REFERENCE** 12 and **Note** 2 is carried out using the standard k-ε model with the wall boundary conditions of the log law type. The experimental apparatus is constructed from ceramics fiber boards measuring 1.7 m × 1.7 m × 3 m (height H) for the wall and 1.0 m × 1.0 m for the floor. A diffusion flame burner fueled by propane gas and dimensioned 0.1 m × 0.1 m × 0.03 m (H) is mounted on the floor. The edge length of the square fire source D is set at 0.1 m. With a fire heat release rate of 15 kW, the present computer simulation considers the following three fire source locations **[Note** 1] which are altered relative to the wall: 1) the fire source is at the corner wall, i.e., $S/D = 0.0$, 2) slightly off the corner, S/D = 0.5, and 3) twice the size of fire D away, $S/D = 2.0$. The computational condition is listed in **TABLE** 1. Simulated cases, presented in **TABLE** 2, are also summarized below.

TABLE 1 Computational Conditions for Corner Plumes

Fire Source Size	Square Fire Source with Edge Length D 0.1 m
Fire Heat Release Rate	Q = 10.5 kW = 10.5 kJ/s (Convection component, equivalent to 70 % of the total heat generation, 15 kW, is assigned on the floor as the heat flux. 70 % is empirically estimated from related experiments.) $w = Q/(\rho \cdot Cp \cdot \Delta T \cdot D^2)$ m/s, $u = v = 0$ m/s, ΔT = 800 K Incompressible: w = 1.09 m/s, k = 0.0713 m^2/s^2, ε = 0.0171 m^2/s^3 (ρ and Cp : at the room temperature) C8S1: k = 0.0713 m^2/s^2, ε = 0.171 m^2/s^3 C8S3: k = 0.0178 m^2/s^2, ε = 0.00216 m^2/s^3 C8S2: 0.0713 , 0.00171 , C8S4: 0.1604 , 0.0578 Simplified Compressible: w = 3.56m/s, k = 0.760 m^2/s^2, ε = 0.596 m^2/s^3 **[Note 6]**
Turbulence Model	Standard k-ε Model 3D, Cartesian Coordinates, Incompressible: Boussinesq Approximation Simplified Compressible: Variable ρ (p = constant)
FDM Scheme for Advection	Terms First-order Upwind (u, v, w, k and ε throughout)
Mesh Division	Meshes A ("coarse"), B ("fine"), C ("dense") **[FIGURE** A-2]
Boundary Conditions	Top: Pressure (Free In/Outflow), Floor and Walls: Velocity – Log law Initial and Ambient Temperatures: 20 °C, Wall Heat Transfer: Insulated
Computational Condition	Unsteady calculation for both incompressible and simplified compressible flows **[Note** 7]
CFD Code	STAR-CD 3.050a (standard k-ε model of Viollet type)

TABLE 2 Computed Cases for Corner Plumes

Case No.	Model	S/D [**Note**1]	Mesh*	Note
C1	Incomp.	0.0	A	
C2	Incomp.	0.5	A	
C3	Incomp.	2.0	A	
C4	Simp.Comp.	0.0	A	Comparison with compressbile flow
C5	Simp.Comp.	0.5	A	
C6	Simp.Comp.	2.0	A	
C7	Incomp.	0.0	B	
C8	Incomp.	0.5	B	
C8S1	Incomp.	0.5	B	ε at fire source: 10 × C8
C8S2	Incomp.	0.5	B	ε at fire source: 0.1 × C8
C8S3	Incomp.	0.5	B	k at fire source: 0.25 × C8
C8S4	Incomp.	0.5	B	k at fire source: 2.25 × C8
C9	Incomp.	2.0	B	
C10	Incomp.	0.0	C	Refinement near the fire source
C11	Incomp.	0.5	C	
C12	Incomp.	2.0	C	

* For a constant S/D ratio, Mesh B refines a near-corner zone of Mesh A, while Mesh C further refines a near-fire area of Mesh B: see **FIGURE** A-2.

Throughout the present study, the walls are assumed to be thermally insulated. Examination of heat conduction across the wall reveals that a heat loss is only almost 1 % of the total heat generated [see **Note** 4]; hence, treating the walls as a thermal insulator would not lead to significant errors.

3.1 Comparative Study of the Compressible and Incompressible Flows

The incompressible flows are solved in C1 – C3, while a simplified compressibility approach under the assumption of variable density and constant pressure is adapted in C4 C6 for comparison. The mesh system employed is Mesh A presented in **FIGURE** A-2: see **Note** 5. The turbulence model used here is based on the standard k-ε model which is implicitly assumed that the statistics are made with Favre average.

3.2 Effects of Mesh Refinement in the Vicinity of Fire

With practical application of CFD prediction for indoor smoke movement in mind, additional cases are computed by further refining meshes to compare results.

Mesh Refinement Near Fire 1: Based on Mesh A ("coarse"), refinement is applied to a zone near the corner. This mesh is called Mesh B ("fine") [**Note** 5]. Incompressible flow analysis is performed for S/D = 0.0, 0.5 and 2.0 (C7 – C9).

Mesh Refinement Near Fire 2: Region near the fire is further refined from Mesh B and named Mesh C ("dense") [**Note** 5]. As above, incompressible flow analysis is made, i.e., C10 – C12.

3.3 Effects of Incoming k and ε at the Fire Source

For C8 using Mesh B, the length scale of turbulence l is set to 0.1D (called C8S1) and 10D (C8S2) and the fluctuating velocity is taken 10 % of the mean velocity w (C8S3) and 30 % (C8S4), thereby effects of the incoming k and ε are examined for the four cases.

4. COMPUTED RESULTS

FIGURE 1 shows comparison of the present numerical results with the measurement [**Note** 2] in the distributions of temperature and velocity for S/D = 0.0. Similarly, **FIGURES** 4 represents results for S/D = 0.5: experimental data and numerical results are also plotted for comparison in **FIGURES** 2 & 3. Similarly **FIGURES** 5 represents results for S/D=2.0.

4.1 Discussion 1: Comparison of the Incompressibility vs. Simplified Compressibility Approaches

1) For S/D = 0.0: In **FIGURE** 1(a), the simplified compressibility model, C4, is seen to reproduce a closer result to the experimental data for a high temperature region near the wall at the height H of 0.5 m, or H/D = 5 than the incompressible flow model (C1) computes. (Note that here and hereafter temperature difference from the ambient air is presented as the temperature distribution.) In the near wall region at H = 1.6 m (H/D = 16), both C1 and C4 overshoot the measured data by approximately 45 % and 65 %, respectively. In the velocity distribution shown in **FIGUIRE** 1(b), both numerical results overpredict the experimental value: about 50 % higher in C1 and 65 % in C4 at H = 0.5 m. The discrepancy increases to 70 % and 80 %, respectively, at H = 1.6 m.

2) For S/D = 0.5: The numerically obtained temperature distributions, using the incompressible model C2 and the simplified compressible model C5, shown in **FIGURE** 4(a), do not capture a region of high temperature (> 700 K) at H = 0.3 m (H/D = 3), underpredicting the experimental result. At 1.2 m (H/D = 12), as the high temperature zone shifts toward the wall, the C5 prediction comes closer to the measurement; however, the C2 result is still about 20 % lower. The velocity distribution, **FIGURE** 4 (b), shows good agreement of the C2 prediction with the experimental result at H = 0.3 m, while the peak value of C5 is roughly 20 % higher. At H = 1.2 m, with the peaks approaching the wall similar to the temperature distribution, overestimation by the numerical simulations of the experimental data reaches about 20 % for C2 and 30 % for C5.

3) For S/D = 2.0: In **FIGURE** 5(a), a high temperature (> 350 K) zone does not appear in the numerical results at H = 0.3 m and, hence, both C3 (incompressibility) and C6 (simplified compressibility) underpredict the measurement data. At 0.8 m (H/D = 8) both results, though getting closer to the experimental result, still undershoot the peak value. In the velocity distribution, **FIGURE** 5(b), both C3 and C6 results at H = 0.3 m attain a 20 % higher peak values than the experiment. The peak value of C6 occurs at a location slightly closer to the wall than for C3, and C6 maintains higher temperatures from the peak up to the wall. At H = 0.8 m, the peaks of both C3 and C6 are closer to the wall than the experimental peak, the C6 peak being closer. The extent of overprediction is about 15 % (for C3) and 10 % (for C6).

■ For S/D = 0.0: The Fire is at the Corner.

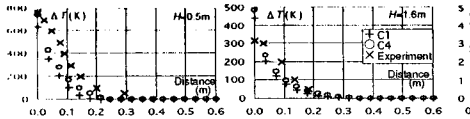

FIGURE 1(a) Comparison of the Temperature Distributions for S/D=0.0 and Mesh A, C1 (Incompressible), C4 (Simplified Compressible) Experiment [see Note2]

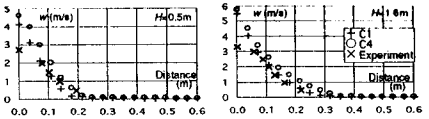

FIGURE 1(b) Comparison of the Velocity Distributions for S/D=0.0 and Mesh A, C1 (Incompressible), C4 (Simplified Compressible) Experiment [see Note2]

■ For S/D = 0.5: The Fire is slightly off the Corner.

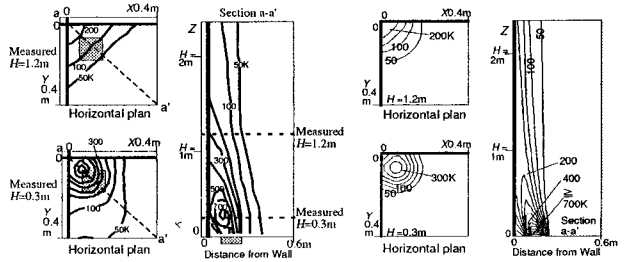

FIGURE 2(a) Experimental Temperature Distribution [see Note 2]

FIGURE 3(a) Temperature Distributions for S/D=0.5 and Mesh A, C2 (Incompressible)

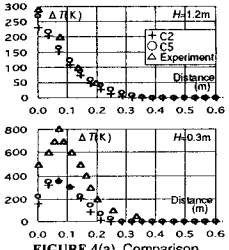

FIGURE 4(a) Comparison of the Temperature Distributions for S/D=0.5 and Mesh A, C2 (Incompressible), C5 (Simplified Compressible) Experiment [see Note2]

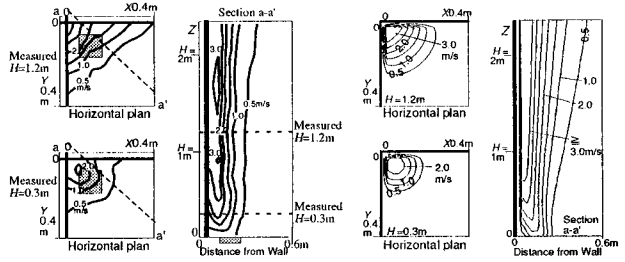

FIGURE 2(b) Experimental Velocity Distribution [see Note 2]

FIGURE 3(b) Velocity Distributions for S/D =0.5 and Mesh A, C2 (Incompressible)

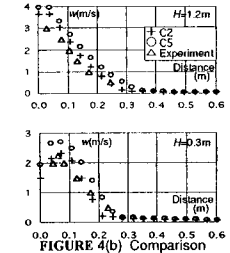

FIGURE 4(b) Comparison of the Velocity Distributions for S/D=0.5 and Mesh A, C2 (Incompressible), C5 (Simplified Compressible) Experiment [see Note2]

■ For S/D = 2.0: The Fire is Located at a Distance Twice the Source Size from the Corner.

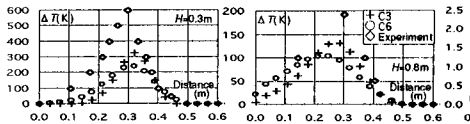

FIGURE 5(a) Comparison of the Temperature Distributions for S/D = 2.0 and Mesh A, C3 (Incompressible), C6 (Simplified Compressible) Experiment [see Note2]

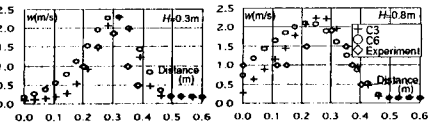

FIGURE 5(b) Comparison of the Velocity Distributions for S/D=2.0 and Mesh A, C3 (Incompressible), C6 (Simplified Compressible) Experiment [see Note2]

■ For S/D = 0.0: The Fire is at the Corner.

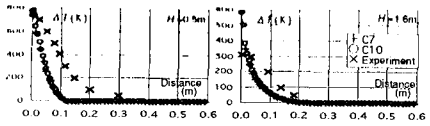

FIGURE 6(a) Comparison of the Temperature Distributions for S/D=0.0, C7 (Incompressible, Mesh B), C10 (Incompressible, Mesh C), Experiment [see Note2]

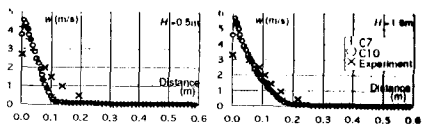

FIGURE6(b) Comparison of the Velocity Distributions for S/D=0.0,C7 (Incompressible, Mesh B), C10 (Incompressible, Mesh C), Experiment [see Note2]

■ For S/D = 0.5: The Fire is slightly off the Corner.

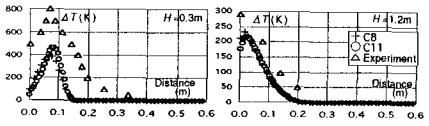

FIGURE 7(a) Comparison of the Temperature Distributions for S/D=0.5,C8 (Incompressible, Mesh B), C11 (Incompressible, Mesh C), Experiment [see Note2]

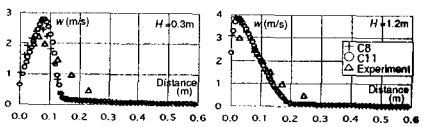

FIGURE 7(b) Comparison of the Velocity Distributions for S/D=0.5,C8 (Incompressible, Mesh B), C11 (Incompressible, Mesh C), Experiment [see Note2]

■ For S/D = 2.0: The Fire is Located at a Distance Twice the Source Size from the Corner.

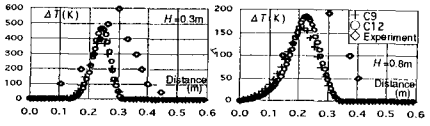

FIGURE 8(a) Comparison of the Temperature Distributions for S/D=2.0,C9 (Incompressible, Mesh B), C12 (Incompressible, Mesh C), Experiment [see Note2]

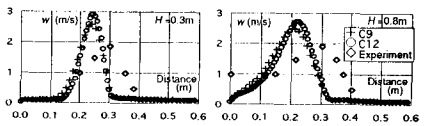

FIGURE 8(b) Comparison of the Velocity Distributions for S/D=2.0,C9 (Incompressible, Mesh B), C12 (Incompressible, Mesh C), Experiment [see Note2]

When the fire is near the wall, e.g., S/D = 0.0 or 0.5, the simplified compressibility model computes higher temperature and velocity right over the source than the incompressible flow model does. When the fire is at the wall, the former predicts the temperature distribution near the flame region better than the latter. The two models give different k and ε distributions, to be discussed later.

4.2 Discussion 2: Effects of Mesh Refinement Near the Fire

FIGURES 6(a) &(b) present comparison of the distribution of temperature and velocity, respectively, between Meshes B ("fine") and C ("dense") for S/D = 0.0. Similarly, Results of S/D = 0.5 are shown in **FIGURE** 7 and for S/D = 2.0 in **FIGURE** 8.

1) For S/D = 0.0: Inspection of **FIGURES** 6(a) &(b) reveals no appreciable difference by the mesh systems, except for the slightly higher peaks in the near-wall temperature and velocity computed in C10 using Mesh C ("dense") compared to the results of C7 (Mesh B—"fine"). In the temperature distribution at 0.5 m (H/D = 5), both C7 and C10 peaks occurring near the wall agree well with the experimental result, while the slopes of the temperature drop of the computed profiles around the peaks are steeper. At 1.6 m (H/D = 16), both C7 and C10 results give respectively 70 % and 100 % higher values than the experimental data. In the velocity distribution, overshoots by C7 and C10 reach 50 % and 65 % at H = 0.5 m, and 60 % and 75 % at H = 1.6 m. For C10, the computed velocity distribution between the peak and the wall is closer to the experimental data than C7. Steeper gradients of the falling velocity profiles around the peaks occur in the computed results than the experimental slope, a similar trend seen previously in the temperature profiles.

2) For S/D = 0.5: In **FIGURE** 7(a), the temperature distribution of C8 (Mesh B, "fine") coincides almost with that of C11 (Mesh C, "dense"). At 0.3 m (H/D = 3), lower peaks—about 50 % for C8 and

40 % for C11 are predicted compared to the experimental data. At 1.2 m (H/D = 12), the results of C8 and C11 again agree well, underpredicting by 25 % of the experimental value. The velocity peaks in **FIGURE** 7(b) exceed the experimental value by 10 and 25 % in C8 and C11, respectively, at H = 0.3 m. At 1.2 m, on the other hand, these computational results almost overlap, giving 25 % higher peaks compared to the measurement. The portions of the computed profiles from the peaks to the wall approach the experimental result. At all heights, the velocity gradients of the numerical simulations are larger than the measured values.

3) For S/D = 2.0: **FIGURE** 8(a) shows no appreciable difference in the temperature distribution for C9 (Mesh B, "fine") and C12 (Mesh C, "dense"). However, the peaks of C12 are about 25 % higher than the C9 data at H = 0.3 m and 20 % at 0.8 m (H/D = 8). Compared to the experimental result, the C9 and C12 peaks occur at locations closer to the walls at all heights. The C12 peaks are about 20 and 5 % lower at H = 0.3 and 0.8 m, respectively than the experimental result. In the velocity distribution, **FIGURE** 8 (b), the results of C9 and C12 differ slightly at all heights: C12 is roughly 15 % higher at H = 0.3 m and, at 0.8 m, 10 % higher than C9. Compared to the experimental result, the C9 and C12 peaks occur at locations closer to the walls at all heights. Compared to the experimental results, the C12 peaks at H = 0.3 and 0.8 m are respectively 50 % and 35 % higher. Again, the computed temperature and velocity decay faster than the corresponding measurement data do.

Under the incompressible flow assumption, peaks manifest accompanying a further steeping of the temperature and velocity profiles around the peaks as the mesh is refined. Especially at lower heights, the peak values of temperature are in better agreement with the experimental result. Although a mesh division dependency is present in the numerical analysis, the mean flows achieve close agreement with the measurement using Mesh A, for which 16 grids are distributed to the fire source.

4.3 Discussion 3: Plume Flow Rate

The flow rate of plume at a given height is defined in **REFERENCE** 12 as the sum of the mass flow rate over a range extending from the location of the maximum temperature rise down to the position where the temperature falls to its 15 % value; thus, it is termed the accumulation flow rate at the 85 % temperature.

This definition, however, causes inconsistency among the numerical and experimental data: in the computed results, an accumulation range of the flow rate becomes narrower since maximum temperatures over the plume attain higher values than those of the experiment for all cases. This will result in an underestimation of the flow rate of computed plumes at high positions where the plume is fully developed, relative to the measurement results and experimental correlations[12] **[Note** 2]. Hence, in the present study, accumulated mass flow rate over a range from the point of the maximum velocity down to where the velocity decays by 99.9 % is defined as the accumulation flow rate at the 99.9 % velocity for compensation purposes. For the correction of the experimental data and the correlations, the formulae proposed by Yokoi[13] for the plume flow rate are adapted. A flow rate that would exist under a 15 % range of the maximum temperature rise is estimated using the formulae giving the velocity and temperature distributions. This amounts to addition of 21 % of the plume flow rate to the original data determined experimentally and from the correlations as supplement. They are termed the corrected experimental flow rate and the corrected correlation flow rate. The accumulation flow rate at the 99.9 % velocity (hereafter simply referred to as "the flow rate" for brevity) of plume is examined in **FIGURES** 9 – 11.

1) For S/D = 0.0: The flow rates for the incompressible flow cases, C1, C7 and C10, presented in **FIGURE** 9 attain higher values than those of the corrected experimental flow rate below 1.9 m height (H/D = 19). For C1 and C7, they are about 30 % higher than the data given by the corrected correlation flow rate, but in good agreement with the corrected experimental flow rate at 2.4 m (H/D = 24). For C10, it is about 5 % lower than the corrected experimental flow rate at H = 2.4 m. At the same height, the simplified compressibility result, C4, gives a 10 % higher flow rate compared to the result of C1. Note that both cases are computed on the same mesh system, Mesh A ("coarse").

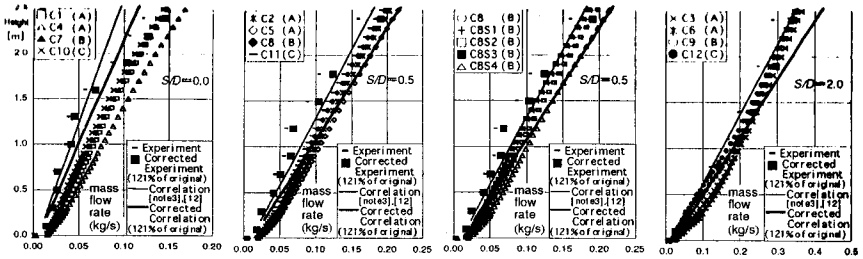

FIGURE 9 Plume Flow Rate for S/D=0.0

FIGURE 10 Plume Flow Rate for S/D=0.5

FIGURE 11 Plume Flow Rate for S/D=2.0

2) For S/D = 0.5: As seen in **FIGURE** 10(a), the flow rates for C2, C8 and C11—the incompressibility results—exceed the corrected experimental flow rate below 1.8 m (H/D = 18). At H = 2.4 m, it is about 10 % lower than the corrected experimental flow rate. There, the simplified compressibility approach, C5, computes an about 7 % higher value than C2 on the same mesh (Mesh A).

3) For S/D = 2.0: On the same Mesh A, the incompressible flow C3 and the simplified compressible flow C6 generate almost identical flow rates below 1.4 m height (H/D = 14), as seen in **FIGURE 11**. Both results give a 30 % higher value than the corrected experimental flow rate at 0.5 m (H/D = 5). The result for Mesh B ("fine"), C9, agrees well with that of C12 using Mesh C ("dense") under the same incompressible flow assumption. At H = 2.4 m, although C3, C6, C9 and C12 generate roughly 20 % lower flow rates compared to the corrected correlation flow rate, they are all in good accord with the corrected experimental flow rate.

4) The incompressible flow results C8S1 – C8S4: As shown for H = 2.4 m in **FIGURE** 10(b), the flow rates of C8S1 and C8S3 are respectively 5 and 7 % lower than the corrected experimental flow rate, while those of C8S2 and C8S4 are 1 and 7 % higher. In all the cases, deviations are within ±7 % of the corrected experimental flow rates.

Under the incompressible flow condition, the mesh dependence of results is not appreciable for the cases C1 – C3, C7 – C9 and C10 – C12. The flow rates show some discrepancies from the corrected correlation flow rate at H = 2.4 m but the differences from the corrected experimental flow rate are less than 5 %. As the distance between the fire source and the wall increases in the order of S/D = 0.0, 0.5 and 2.0, the plume flow rates at any height also increase. When the flow rate ratios are calculated using the value at H = 2.4m as reference, they become 1, 1.3 and 2.4, in good agreement with the corrected experimental flow rate. Based on these results, the standard k-ε model can in practice provide satisfactorily accurate predictions for estimating the flow rate of corner plumes.

4.4 Discussion 4: Distribution of k and ε

1) Effects of Meshes: **FIGURE** 12 (a) &(b) depict the distribution of k and ε along the plume central axis [see **Note** 8] for S/D = 0.5: flows in C2, C8 and C11 are incompressible, while C5 solves the simplified compressible flow. For the three incompressible flow results, k does not vary significantly roughly over H=1.0 m (H/D = 10).

2) Comparison of the Incompressible and Simplified Compressible Models: In the simplified compressibility result, C5, both k and ε increase rapidly from right above the fire source and they attain maxima at about H = 0.01 to 0.15 m, or H/D = 0.1 – 1.5. Over H = 1.0 m, k in C5 differs little from C2, C8 and C11 computed for the incompressible flow.

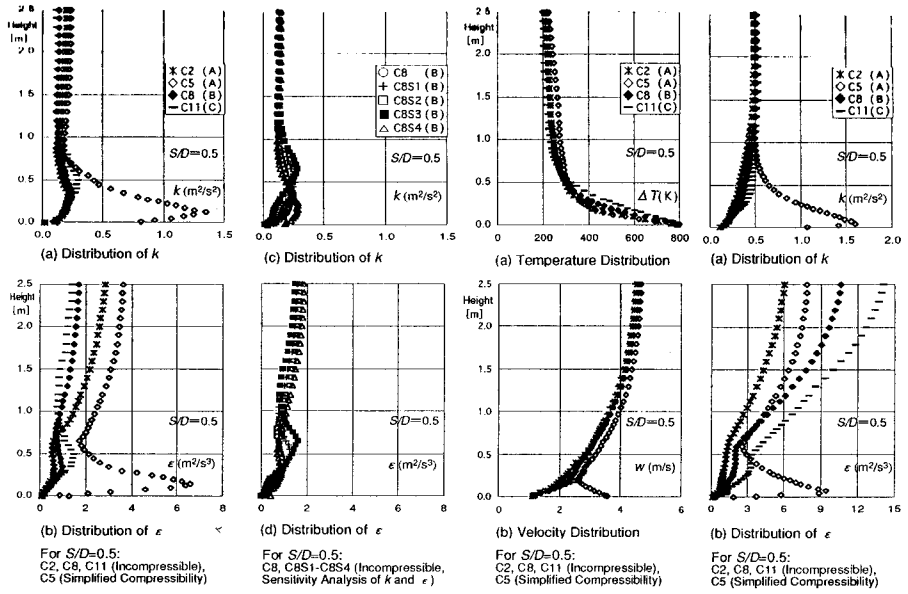

FIGURE 12 Distributions of k and ε along the Plume Central Axis [see Note 8]

FIGURE 13 Distributions of Temperature and Velocity along the Plume Central Axis

FIGURE 14 Vertical Distributions of k and ε Maxima

3) Effects of the Inflow Values of k and ε at Fire: **FIGURES** 12 (c) & (d) display the distributions of k and ε along the plume central axis for C8S1 – C8S4 having various inflow values for k and ε. As seen, although the peak heights for k or ε differ slightly among the results, no appreciable difference appears over H = 1.0 m. Only the distributions in k and ε right above the fire are affected by their incoming values. Beyond that, however, effect is insignificant, as the small differences of the results demonstrate.

4) Distribution of the k and ε peaks in the Simplified Compressibility Simulation: **FIGURE** 13 represents the temperature and velocity distributions along the plume central axis for S/D = 0.5, while **FIGURE** 14 shows the distribution of the k and ε maxima as a function of height. In a lower portion of plume near the fire source, significant temperature decay takes place. In the simplified compressibility simulations, this results in a rapid contraction of the air in the region, which in turn increases gradients of the vertical velocity w. This causes a large Pk, the production term of k [see **Note** 9], increasing k and ε by five- to ten-fold values of the incompressible flow results. There is, however, little difference in the computed eddy kinetic viscosity ν_t between the two flow models, keeping close agreement of the temperature and velocity distribution in lower portions of the plume between the two results.

5. CONCLUSIONS

1. The plume near the corner is simulated numerically using the standard k-ε model to investigate the effects of the incompressibility and the simplified compressibility by comparing the results with the experimental data. When the fire source is located near the wall (S/D = 0.0 or 0.5), the simplified compressibility results attain higher temperature and velocity right above the fire than the incompressibility results. When the fire is at the wall, the former reproduces the measurement data more closely than the latter.

2. The computational mesh near the fire location is refined to examine the accuracy against the experimental data. In incompressible flow, the peaks of temperature and velocity manifest with mesh

refinement. In particular, the temperature peaks occurring at lower levels come to better agreement with the experimental results. Although the numerical solutions are mesh dependent, the mean flow may be simulated satisfactorily well using 16 meshes in the fire source.

3. The accumulation flow rates at the 99.9 % velocity computed on Meshes A, B and C differ little, within 5 % deviations at 2.4 m height ($H/D = 24$). As the fire source is positioned further away from the wall in the S/D order of 0.0, 0.5 and 2.0, the plume flow rate increase at any height. For these S/D's, the flow rate ratio is calculated to be 1, 1.3 and 2.4, almost identical values with the corrected experimental flow rate at 2.4m height. Hence, the performance of the standard k-ε model for the corner plume situations is satisfactory.

4. The inflow values of k and ε are varied at the fire source. When the fluctuating velocity is modified over a range of ±10 % about the original data and the length scale of turbulence is set at either 0.1 or 10 times the original, fluctuations in the accumulation flow rate at the 99.9 % velocity change within ±7 % about the unmodified value. In the k and ε distributions, the inflow values of k and ε exert influences right above the fire but the effects are far smaller beyond that height. Beyond the fire, there is little change in the distribution of k arising from the differences in the flow models, i.e., incompressible and simplified compressible, and the mesh systems.

From the practical standpoints for the numerical simulation of corner plumes considered above, sufficiently accurate predictions using the incompressible form of the standard k-ε model can be obtained on (1) Mesh B, in which the fire source is divided into 64 meshes, if the accuracy is of concern within a bound of realistic computational requirement, and (2) Mesh A (16 meshes for the fire), if qualitative assessment is of the main interest.

ACKNOWLEDGMENT

The authors are grateful to Professor Osami Sugawa of the Center for Fire Science and Technology, Science University of Tokyo, who provided the experimental data of **REFERENCE** 12.

NOTES

1) **Location of Fire Source :** As shown in **FIGURE** A-1, suppose $S1$ and $S2$ measure the distances between each wall and the square fire source of edge length D. The location of the fire is expressed in terms of ratio S/D, where S is the reference length defined as $S=\sqrt{S1 \cdot S2}$ [11]

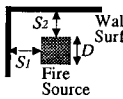

FIGURE A-1 Geometrical Relationship between the Fire Source and the Walls

2) Plume Experiment of Sugawa: Obtained through personal communication November 1997.

3) Experimental Correlation for Corner Plume: The mass flow rate of plume in a region under the influence of wall can be written using a coefficient Cm for S/D as [12]

$$mp = k' Q^{1/3}(Z+Z0)^{1.0} \quad Z0 = B(Af)^{1/2} \quad B = 1.5 \pm 0.3 \quad k' = Cm(\rho_\infty^2 g/(C_p T_\infty))^{1/3}$$

For $S/D = 0.0$, set $Cm = 0.04$; for $S/D = 0.5$, $Cm = 0.075$; and, for $S/D = 2.0$, $Cm = 0.145$

B is set at 1.5 in the above equations for the data shown in **FIGURES** 9 – 11.

4) Wall Heat Conduction: The experiment employs ceramics fiber boards of a 25 mm thickness. Measurements of temperature and upward velocity are started 5 minutes after the burner is ignited. For $S/D = 0.0$, heat transfer to the wall is estimated to be about 1 % of the total heat generation from based on temperature measurements taken near the wall. Hence, it may be safe to state that treating the wall as thermal insulators would introduce only small errors in the simulation results.

5) Computational Mesh:

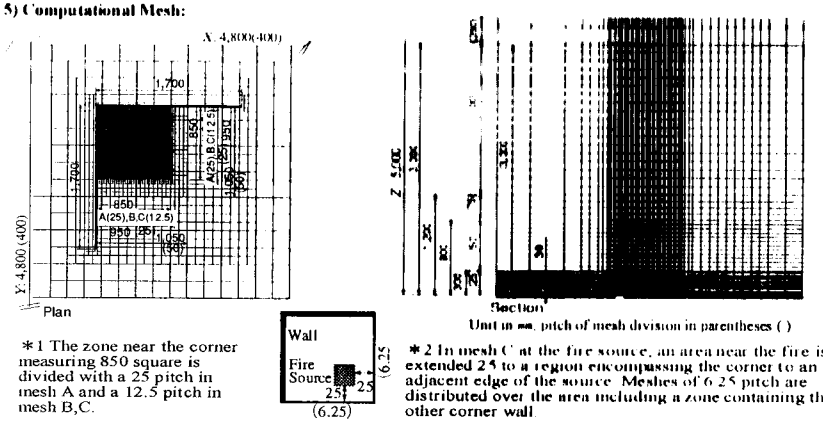

*1 The zone near the corner measuring 850 square is divided with a 25 pitch in mesh A and a 12.5 pitch in mesh B,C.

*2 In mesh C at the fire source, an area near the fire is extended 2.5 to a region encompassing the corner to an adjacent edge of the source. Meshes of 6.25 pitch are distributed over the area including a zone containing the other corner wall.

FIGURE A-2 Computational Meshes A*1, B*1, C*1, *2

6) Determination of k and ε : For the k and ε values, k is set *via* a fluctuation velocity equivalent to 20 % of w, while ε is calculated from the formula below, in which the fire length D is taken as the length scale of turbulence l:

$$\varepsilon = (0.09 \times k^{3/2})/l = (0.09 \times k^{3/2})/D$$

7) Time Step for Unsteady Computations: As an effective means to reach the steady-state solution, small time step values between 0.001 and 0.01 s are assigned in the initial stage until the computation becomes stable; then, the time steps are progressively increased.

8) Distribution of k and ε along the Plume Central Axis: In the horizontal cross section at a given height, the point at which w reaches a maximum is determined as the location of the plume axis. Values of k and ε at these positions are plotted in the results.

9) The Production and Buoyancy Force Terms in the Transport Equation of k: In the transport equation of k, Eq. (1), the production term Pk and the buoyancy force term Gk are expressed as in Eqs. (2) and (3), respectively, while the diffusion term Gk is modeled in the k equation as in Eq. (5):

$$\frac{\partial k}{\partial t} + \frac{\partial u_i k}{\partial x_i} = \frac{\partial}{\partial x_i}\left(\frac{\nu_t}{\sigma_k}\frac{\partial k}{\partial x_i}\right) + (P_k + G_k) - \varepsilon \quad \cdots\cdots(1)$$

$$Pk = \nu_t\left(\frac{\partial u_i}{\partial x_j} + \frac{\partial u_j}{\partial x_i}\right)\frac{\partial u_i}{\partial x_j} \quad \cdots\cdots(2)$$

$$Gk = -g\beta\frac{\nu_t}{\sigma_t}\frac{\partial T}{\partial z} \quad \cdots(3) \qquad \nu_t = C_t\frac{k^2}{\varepsilon} \quad \cdots(4)$$

$$\frac{Dk}{Dt} = Dk + Pk + Gk - \varepsilon \quad \cdots\cdots(5)$$

$C1 = 1.44$, $C2 = 1.92$, $C3 = 0.0$, $G_t = 0.09$

NOMENCLATURE

Af	fire source area [m²]
Cp	specific heat [kJ/kg·K]
D	edge length of fire source [m]
g	gravitational acceleration [m/s²]
H	height[m]
k	turbulent kinetic energy [m²/s²]
k', B, Cm	coefficients
l	length scale of turbulence [m]
mp	mass flow rate of plume [kg/s]
$mco2$	CO2 mass flow rate of plume [kg/s]
Q	heat release rate [kJ/s]
S	distance between fire source and wall [m]
T	temperature [K]
ΔT	temperature difference [K]
t	time [s]
X,Y,Z	x,y,z coordinate [m]
xi	position of i coordinate [m]
u, v, w	velocity components in the X, Y and Z directions [m/s]
ui	velocity component in the xi direction[m/s]
Z	height [m]
$Z0$	height of virtual origin from top of combustible [m]

Greek letters

β	coefficient of expansion [1/K]
ε	dissipation rate of turbulent kinetic energy [m²/s³]
ρ	density [kg/m³]
ν_t	eddy visicosity [m²/s]
σ	Prandtl number

Subscript

∞	ambient condition

REFERENCES

1. Hara, T., Yokoi, M. and Kato, S., "Study on Thermal Plumes in Free Space by Means of Numerical Simulation Based on Standard k-ε Model", J. Archit. Plann. Environ. Eng., AIJ, No.530, Apr., 2000

2. Hara, T., Yokoi, M. and Kato, S., "Analysis of Thermal Plumes with Numerical Simulation Part5, Influence of Heat Conduction through Walls on Numerical Solution of Corner Plumes ", Summaries of Technical Papers of Annual Meeting, Architectural Institute of Japan, pp. 145~146, Sept., 1999

3. Hara, T., Yokoi, M. and Kato, S., "Analysis of Thermal Plumes with Numerical Simulation and Experimental Results Part4, Influence of Mesh Division on Numerical Solution to Corner Plumes", Proceedings of Annual Meeting of JAFSE, pp.396~399, May, 1999

4. Yokoi, M., Hara, T. and Kato, S., "Analysis of Thermal Plumes with Numerical Simulation and Experimental Results Part3, Influence of Numerical Scheme, Compressible Model and Incompressible Model on Numerical Solution", Proceedings of Annual Meeting of JAFSE, pp.392~395, May, 1999

5. Cetegen, B.M., Zukoski, E.E. and Kubota, T., NBS-GCR-82-402, Entrainment and Flame Geometry of Fire Plumes, U.S. Department of Commerce, National Bureau of Standards, pp. 63,74~75,Aug., 1982

6. Klote, J. H., Milke, J. A., Design of Smoke Management Systems, American Society of Heating, Refrigerating and Air-Conditioning Engineers, Inc., pp.110~111,1992

7. Takahashi, W., Sugawa, O. and Nara, M., "Properties of a Corner Fire", Proceedings of Annual Meeting, JAFSE, pp.84~87, May, 1994

8. Tanaka, H., Takahashi, W., Nara, M., Sugawa, O. and Segawa, R., "Flame Height Behavior in and beside a Corner", Summaries of Technical Papers of Annual Meeting, Architectural Institute of Japan, pp.1379~1380, Sept., 1994

9. Takahashi, W., Sugawa, O. and Tanaka, H., "Properties of Flame/Plume Behavior in and near a Corner", Summaries of Technical Papers of Annual Meeting, Architectural Institute of Japan, pp.45~46, Aug., 1995

10. Takahashi, W., Sugawa, O. and Ohtake, M., "Flame and Plume Behavior in and near a Corner of Wall", Proceedings of Annual Meeting, JAFSE, pp.306~307, May, 1997

11. Sugawa, O., Takahashi, W., Ohtake, M. and Satoh, H., "A Study on Fire Characteristics in a Tall and Narrow Atrium", International Symposium on Fire Science and Technology,1997

12. Tobari, T., Sugawa, O., "Flame Behavior in and near Room Corner", Proceedings of Annual Meeting, JAFSE, pp.326~329, May, 1999

13. Yokoi, S., "Study on the Prevention of Fire-Spread Caused by Hot Upward Current", Report of the Building Research Institute, No.34, Nov., 1960

14. Murakami, S., Kato, S. and Suyama, Y., "Analysis of Finite Difference Schemes for Convective Terms such as Quick Scheme or Other Schemes, Study on Diagnostic System for Numerical Simulation of Turbulent Flow in Room (Part2)", J. Archit. Plann. Environ. Eng., AIJ, No.390, pp.1~12, Aug., 1988

15. Murakami, S., Kato, S. and Nagano, S., "Estimation of Error Caused by Coarseness of Finite-Differencing, Study on Diagnostic System for Simulation of Turbulent Flow in Room (Part1)", J. Archit. Plann. Environ. Eng., AIJ, No.385, pp.9~17, Mar., 1988

A Numerical Study of Smoke Movement in Atrium Fires with Ceiling Heat Flux

J.Y. JEONG, H.S. RYOU, S.C. KIM and C.I. KIM
Department of Mechanical Engineering, Chung-Ang University
221 Huksuk-Dong, Dongjak-Ku, Seoul 156-756, Korea

ABSTRACT

This paper describes the smoke filling process of a fire field model based on a self-developed SMEP(Smoke Movement Estimating Program) code to the simulation of fire induced flows in the two types of atrium space containing a ceiling heat flux. The SMEP using PISO algorithm solves conservation equations for mass, momentum, energy and species, together with those for the modified k- epsilon turbulence model with buoyancy term. Compressibility is assumed and the perfect gas law is used. Comparison of the calculated upper-layer average temperature and smoke layer interface height with the zone models has shown reasonable agreement. The zone models used are the CFAST developed at the Building and Fire Research Laboratory, NIST, U.S.A. and the NBTC one-room of FIRECALC developed at CSIRO, Australia. For atrium with ceiling glass the consideration of the ceiling heat flux by solar heat may be necessary in order to produce more realistic results. The smoke layer interface heights that are important in fire safety were not as sensitive as the smoke layer temperature to the nature of ceiling heat flux condition. This study highlights the utility of SMEP field modeling for the analysis of smoke movement and temperature in atrium fires.

KEY WORDS: Smoke filling process, heat flux, SMEP, Atrium, Field model, Zone model

INTRODUCTION

In recent years, the atrium building has become commonplace. Other large open spaces include enclosed shopping malls, arcades, sports arenas, exhibition halls and airplane hangers. The smoke generated from fires in these spaces may cause people to panic and interfere with evacuation. Not only does the smoke generated from modern synthetic materials lead to disorientation and death of the occupants, but also large quantities of smoke become an obstacle to fire extinction. Therefore fire safety is an important issue to be considered by architects and engineers when they design the fire protection systems such as sprinklers and smoke control systems etc. However, there are few design guides with strong scientific backgrounds suitable for use by the construction industry.

The ability of sprinklers to suppress fires in spaces with ceilings higher than 11 to 15m is limited[1,2]. Because the temperature of smoke decrease as it rises(due to entrainment of ambient air), smoke may not be hot enough to activate sprinklers mounted under the ceiling of